[AMERICAN JOURNAL OF SCIENCE, VOL. 282, OCTOBER, 1982, P. 1151-1183]

American Journal of Science

OCTOBER 1982

PYRITE AND SIDERITE FORMATION IN BRACKISH AND FRESHWATER SWAMP SEDIMENTS

DIEKE POSTMA

Institute of General Geology, Øster Voldgade 10,
DK-1350 Copenhagen K, Denmark

ABSTRACT. Siderite and pyrite are found in large amounts and spatially well-separated in Skjernå delta swamp sediments. Small amounts of vivianite are found associated with siderite. Siderite occurs as loose aggregates of microcrystalline carbonate, while pyrite is present dominantly as framboids. Vivianite is mostly found as very small crystallites with the occasional occurrence of large crystals.

Siderite is associated with freshwater sediments, while pyrite is found in brackish water sediments. This conclusion is based on sedimentological data as well as on analyses of chloride concentrations in the pore waters. The distribution of siderite and pyrite in fresh and brackish water sediments can be explained satisfactorily by a simple equilibrium model. Qualitatively, this model is supported by sulfate/sulfide and Fe^{2+} concentrations in the pore water. Calculated saturation states of the pore water for siderite show that, in general, pyritic sediments are subsaturated, whereas sideritic sediments are supersaturated. However, in some pyritic sediments the solubility product for siderite is exceeded, below the level where sulfate reduction is complete, although no siderite could be detected.

Vivianite is found together with siderite in freshwater sediments. The freshwater sediments contain much higher phosphate concentrations than brackish water sediments while the reverse is found in the pore waters. This, together with high degrees of supersaturation for vivianite in the freshwater sediments, provides evidence for ongoing vivianite precipitation.

INTRODUCTION

Pyrite and siderite are two of the most common authigenic iron minerals found in ancient sediments (for example, Curtis, 1967; Pearson, 1979). Both minerals are usually found in fine-grained sediments with a significant content of organic matter. While the conditions for their formation can be characterized qualitatively by thermodynamic equilibrium calculations (Berner, 1964; Garrels and Christ, 1965), a study of recent equivalents is also necessary for a sound interpretation of their paleoenvironmental significance. A great amount of work has been done on the formation of pyrite in recent sediments (for example, Berner, 1970; Sweeney and Kaplan, 1973; Goldhaber and Kaplan, 1974; Rickard, 1975; Howarth, 1979). Much less information is available on recent siderite

formation, although it is reported in an increasing number of studies (Bricker and Troup, 1975; Anthony, 1977; Suess, 1979; Postma, 1977, 1981).

This paper contains a study of recent swamp sediments in which both siderite and pyrite are currently being formed. The area studied is within the Skjernå delta, a small recent delta complex (about 40 km^2) situated on the eastern side of the Ringkøbing fjord, Denmark.

The Ringkøbing fjord is at present brackish but has varied considerably in salinity during recent times. The delta is protected at the sea side by a coastal sand barrier behind which organic-rich swamp sediments, with a maximum thickness of up to 10 m, have accumulated. The swamp sediments vary in composition from Phragmites peat, with different amounts of clay and silt, to wood peat and gyttja, all occurring in a complex interfingering system. The sediments and their distribution are described in detail by Halaburt (in preparation). The sediments generally have a very high content of organic matter (fig. 1) and a virtual absence of $CaCO_3$. Ca-concentrations in sediments (aqua regia soluble) are generally less than 1.5 percent dry weight.

During the late sixties, the area was reclaimed for agricultural purposes, and at present the groundwater level varies seasonally from surface level to about 1 m in depth.

The aim of the present study is to describe the distribution of pyrite and siderite in the sediments and to relate their formation to the depositional environment and the pore water chemistry of the deposit. Oxidation processes will be dealt with elsewhere (Postma, 1982).

METHODS

Sediments were studied, with divergent intentions, from two types of borings. The first type of boring was aimed at mapping the distribution of total sulfur and aqua regia-soluble-iron in the sediments. These borings were made with various bog coring devices. The position of the redoxcline was determined by field Eh/pH measurements with a portable pH-meter. Sediment samples were frozen in the field and transported in this state to the laboratory. The samples were subsequently freeze-dried and used for chemical analysis and X-ray diffraction.

Chemical analysis of the sediment samples included determination of total S, total C, and aqua regia soluble Fe and Ca. Total S was determined by combustion in a LECO induction furnace equipped with an automatic SO_2 titration unit. Pure pyrite was used as a standard. Total C was also determined by combustion in the induction furnace. The evolved CO_2 was measured gravimetrically by absorption on ascarite. Aqua regia soluble Fe and Ca were analyzed with flame AAS.

The second type of boring was aimed at supplying information on pore water chemistry and the distribution of different iron and sulfur compounds in the sediments. These borings were carried out using a "Stade" sampler. This sampler recovers cores within PVC sleeves which can be sealed immediately after recovery in order to prevent admission of air. Pore water analysis for oxidation- and degassing-sensitive compo-

nents was done in the field using a laboratory-equipped van.

The procedures have been described in detail by Postma (1981) and are summarized only briefly here. Cores within their PVC sleeves are placed in a N_2-filled glove box. Samples are taken by opening the PVC sleeve and extracting the pore water with a Reeburgh type sediment squeezer through 0.45 μm membrane filters. Still within the glove box, pH is measured, alkalinity titrated, and reagents added for colorimetric analysis of H_2S, Fe^{2+}, and PO_4-P. The sediments were frozen in the field and stored for later analysis.

Chemical analyses of the sediments for different S and Fe fractions were carried out on the frozen filter cakes. The water content was determined by freeze-drying separate portions of sediment.

Acid volatile sulfide was determined by boiling portions of the frozen sediment with 1 N HCl. The evolving H_2S was trapped in a silver nitrate solution and weighed as silver sulfide (Goldhaber and others, 1977).

This method gives only a minimum estimate for the content of acid volatile sulfides, as any Fe(III) present may oxidize the evolving H_2S to

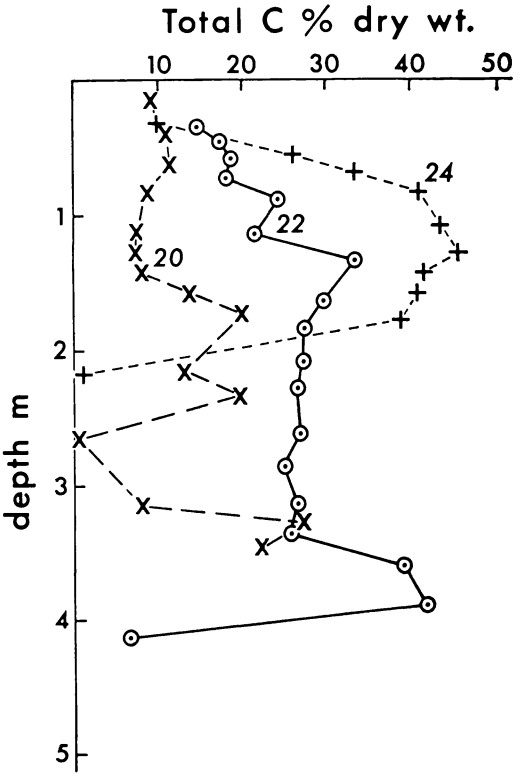

Fig. 1. Total carbon in sediments of borings 20, 22, and 24. The locations of these and other borings are given in figure 10.

elemental sulfur (Pruden and Bloomfield, 1968; Berner, 1974). Addition of $SnCl_2$ to the sample prevents oxidation of H_2S (Pruden and Bloomfield, 1968; Berner, Baldwin, and Holdren, 1979) but causes instead a slow reduction of pyrite (Pruden and Bloomfield, 1968 and tests in this laboratory), and results may therefore overestimate the acid volatile sulfide content.

In sediment samples containing siderite, the analytical procedure for acid volatile sulfide was extended subsequent to the $AgNO_3$ trap with concentrated H_2SO_4 and $CaCl_2$ traps for removing water vapor, after which CO_2 was absorbed on an ascarite/Mg-perchlorate trap. The CO_2 content was then determined gravimetrically. Test runs with mixtures of $Na_2S \cdot 9H_2O$ and $CaCO_3$ showed a recovery for both sulfide and carbonate of 98 percent and over. The sediment suspension was then filtered, and dissolved Fe measured in the filtrate. The iron content is taken as an expression for "reactive iron" and includes iron derived from acid volatile sulfides, carbonates, oxides, and other possible sources.

This expression for reactive iron, although different from that used by Berner (1970) who boiled the samples for 1 min with 12 N HCl, has been adopted because of the large heterogenity of the samples. Subsequent extraction tests with Berner's method showed that less than 10 percent additional Fe was extracted.

After HCl extraction, the sediment was digested overnight with aqua regia, and sulfate was determined gravimetrically in the solution. The SO_4-S measured in this way is attributed to pyrite-S even though it, as discussed in more detail below, includes minor amounts of sulfur from organic sources (Kaplan, Emery, and Rittenberg, 1963; Goldhaber and others, 1977).

PO_4-P was determined in HCl extracts and in aqua regia extracts of bulk samples with the molybdenium blue method (Harwood, van Steenderen, and Kühn, 1969).

For scanning electron microscope (SEM) studies, the sediment was fractionated with heavy liquid to enable isolation of siderite and pyrite, whereas hand-picked material was used for vivianite. The samples were coated with gold or aluminum and run on a Cambridge Stereoscan MK 2 or on a Cambridge Stereoscan S180 equipped with a Link energy dispersive unit.

RESULTS

Mineralogy.—The iron minerals that occur in large amounts in the reduced parts of the Skjernå-delta sediments are pyrite and siderite while vivianite is found in smaller amounts. The three minerals have been identified by both X-ray diffraction and SEM.

Siderite is moreover easily recognized in the field as it occurs as yellowish impregnations of the sediment, while occasionally, concretions are also found. Inspection by SEM shows that siderite is present in the sediments as loose aggregates of elongated carbonate grains (pl. 1-A) with random organization. Each individual carbonate grain is about 2 to 10 μm long, and the carbonate grains are often intergrown (pl. 1-B). Higher

PLATE 1

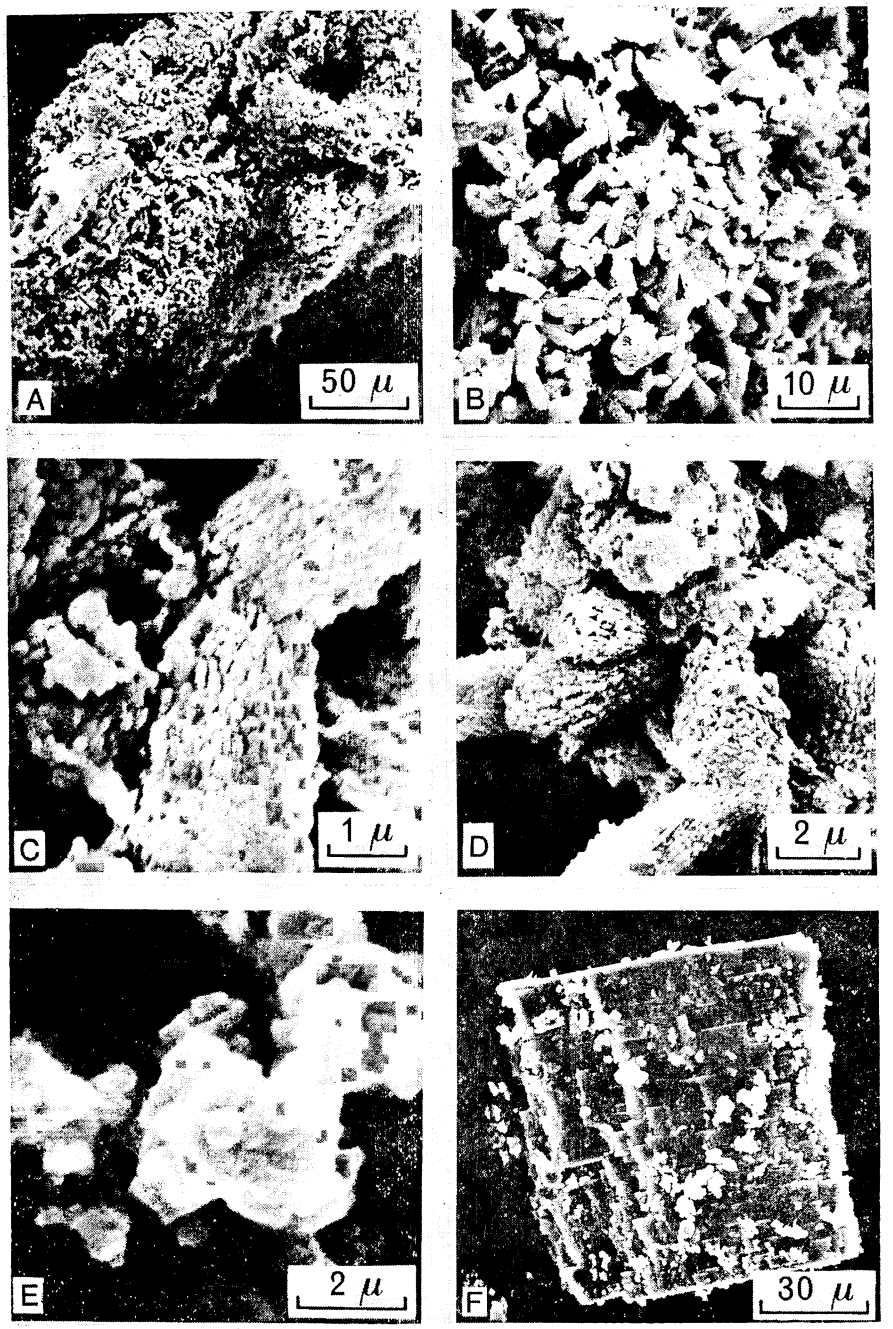

SEM micrographs of siderite and vivianite: (A) an aggregate of siderite grains; (B) elongated siderite grains randomly organized; (C) detail of an elongated siderite grain showing the individual siderite crystals organized in a sheaf-like structure; (D) overgrowth of siderite; (E) small particles containing only P and Fe, which are assumed to be vivianite; (F) part of a exceptionally large vivianite crystal.

magnification reveals that the carbonate grains are not single carbonate crystals but have a complex internal structure. In some cases they consist of elongated siderite crystals apparently organized in sheaves (pl. 1-C) while in other cases they appear to be built up by subsequent overgrowth (pl. 1-D). The grain sizes of the individual siderite crystals are in all cases extremely small and mostly of colloid size. The minimum observed crystal size is definitely below 0.1 μm and seems only to be limited by the maximum resolution of the SEM. The siderite is comparatively pure $FeCO_3$ in contrast to what was found at another locality (Postma, 1981), where extensive solid solution with $MnCO_3$ and $CaCO_3$ occurred. The X-ray unit used in combination with the SEM only showed traces of Mn and Ca in siderite, whereas X-ray diffraction patterns also corresponded to that of pure siderite.

PLATE 2

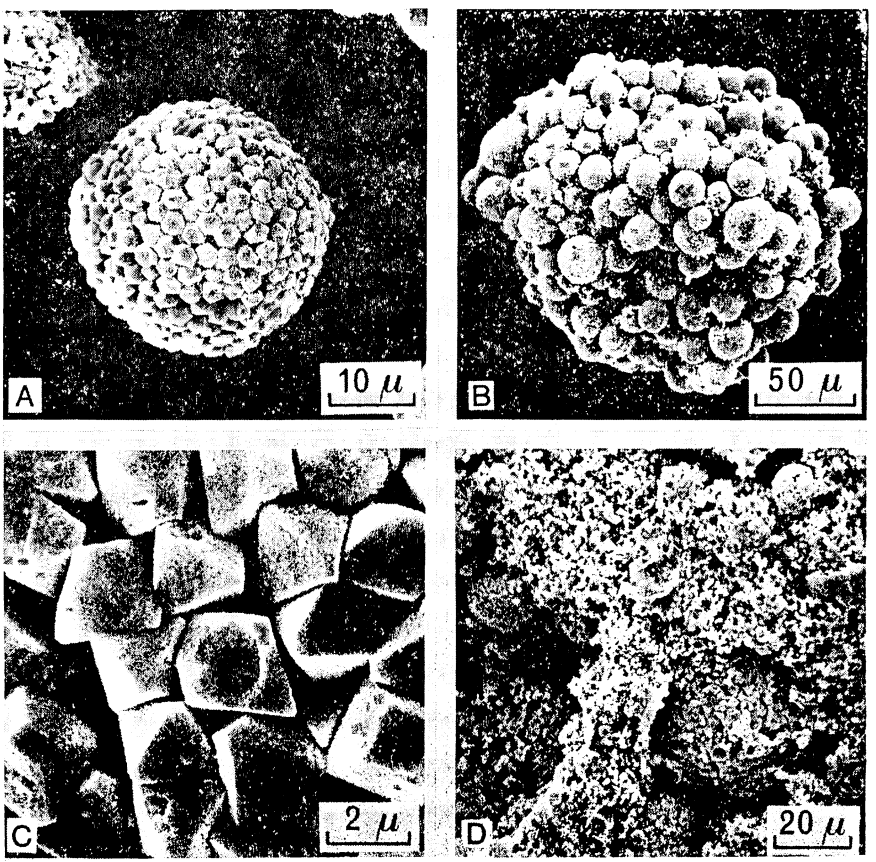

SEM micrographs of pyrite: (A) Framboidal pyrite. The crystal habits are combinations of octahedra and cubes. HCl cleaned material. (B) Polyframboidal pyrite. (C) Octahedral pyrite in a framboid. Note the random organization and the lack of matrix. HCl cleaned material. (D) Growth of non framboidal pyrite on framboidal pyrite.

Vivianite is also easily recognizable in the field as it occurs concentrated as clear white spots in the sediments. Upon exposure to the air, vivianite rapidly turns bright blue due to oxidation of part of the Fe^{2+} within the vivianite crystal lattice (Faye, Manning, and Nickel, 1968) and cannot be missed in this form. Vivianite samples for SEM work were handpicked under a binocular microscope. Although great care was taken to prevent sample oxidation, which can be checked by the color change of vivianite, the short time of exposure to the air during sample preparation for SEM was sufficient for vivianite to turn blue. In order to avoid further sample oxidation, SEM work was always completed the same day sample preparation had taken place.

Recognition of vivianite by SEM is difficult as the vivianite crystals in most cases are extremely small. Even in material that appeared through a binocular microscope as pure, but very fine-grained, vivianite, no crystals of vivianite could be recognized with the SEM. However, using the X-ray unit on the SEM, it was found that grains like those shown in plate 1-E contained only P and Fe and combined with the macroscopic selection, are assumed to be vivianite crystals. Particles with a size of less than 0.1 μm are certainly present, and it would again appear that only the resolution of the SEM limited the observation of even smaller particles. Occasionally, exceptionally large vivianite crystals were observed, an example of which is shown in plate 1-F. The flaky appearance of the crystal is probably due to the partial oxidation of Fe(II) in vivianite (McCammon and Burns, 1980).

The only iron sulfide identified by X-ray diffraction is pyrite. Pyrite is predominantly found as well-developed framboids (pl. 2-A) ranging in size from 2 to 35 μm. Framboids may cluster together and form larger aggregates (pl. 2-B) ranging from 100 to 175 μm, which could be termed polyframboids (Love, 1971). Single crystals within framboids are generally equal in size (6-0.5 μm or less) and have an octahedral crystal habit, although cubes and combinations of both habits also occur. Framboids do not contain any matrix (as reported by Scheihing, Gluskoter, and Finkelman, 1979) and neither have organic "sac's" (Love and Murray, 1963; Sweeney and Kaplan, 1973) been observed. Occasionally polyframboids were found overgrown by pyrite (pl. 2-D). Pyrite was not found disseminated as single crystals in the sediments.

Sediment chemistry.—An environmental study on the origin of iron polluted drainage water within the Skjernå-delta supplied about 350 sediment analyses from 25 borings for total S and aqua regia soluble Fe. This large amount of data revealed a very distinct pattern for the distribution of iron and sulfur in the peat basin of the delta.

In the western part of the peat basin, the only identified iron mineral below the redoxcline is pyrite, and the sediments contain very high concentrations of both iron and sulfur. Values as high as 19 percent S dry weight have been measured in several samples, but the major part shows concentrations in the range of 2 to 12 percent S. The distribution of iron and sulfur as a function of depth is illustrated in boring 23 (fig.

2). Large variations for both iron and sulfur are found and are a general feature. The parallel curves for iron and sulfur in figure 2 suggest a common origin. A plot for boring 14 (fig. 3) from the same area confirms this and shows that contents of iron and sulfur correspond nearly quantitatively to the theoretical ratio in pyrite. This suggests that up to 30 percent of the total sediment weight can be present as pyrite. Although the correlation between iron and sulfur is not in all cases as perfect as found in boring 14, the general trend is very much the same. This is illustrated in a simplified east-west profile through the peat basin (fig. 4), where it is observed that the mole ratio in the whole western part is close to that of pyrite. The increase of the 2 Fe/S ratio above the redoxcline is due to the oxidation of pyrite and the selective removal of pyrite-S as sulfate in solution (Postma, 1982).

In order to gain some insight in the distribution of different forms of iron and sulfur in the sediments, several cores were analyzed in greater

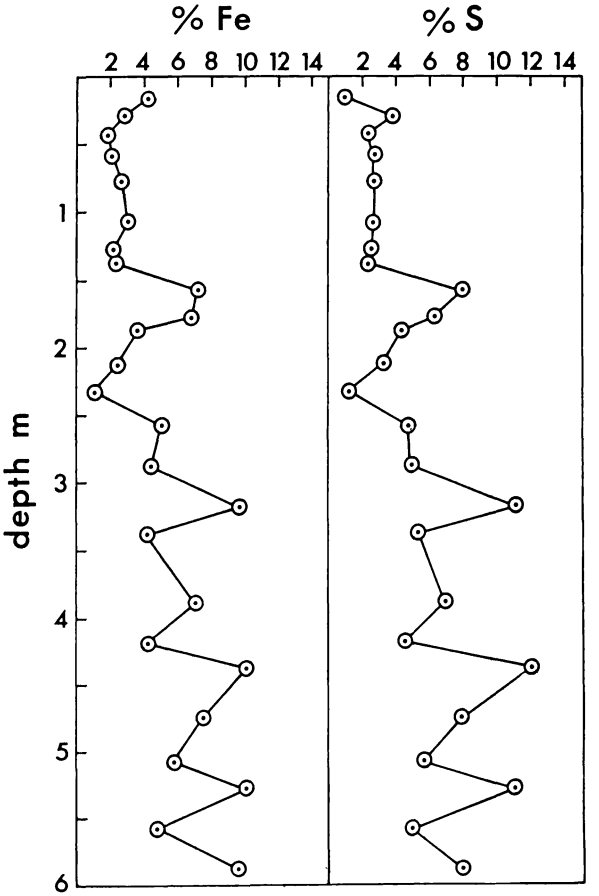

Fig. 2. Total sulfur and aqua regia soluble iron, expressed as percent dry weight, in sediments of boring 23. The position of the redoxcline is at 0.8 m depth.

detail. Results for 2 borings in the pyritic area are shown in figure 5 and table 1.

Not surprisingly, pyrite is the major source for both iron and sulfur. This is in good agreement with the correlation of total sulfur and iron which corresponded to pyrite (fig. 3). Reactive iron, or Fe_{HCl}, is present at a low and rather constant level. In principle, this demonstrates that the sediments have a small but consistent potential for further pyrite formation. This may also be expressed by the degree of pyritization P, as defined by Berner (1970):

$$P = \frac{\%Fe_{pyrite}}{\%Fe_{pyrite} + \%Fe_{HCl}}$$

Calculated values for boring 41 (table 1) and 40 (not shown) range from 0.56 to 0.95 and are in most cases higher than 0.75. Equally high values for P have also been reported from mangrove swamps in Thailand (van Breemen, 1976), but these differ markedly from what is found in coastal marine sediments, where values below 0.5 dominate (Berner, 1970; Jørgensen, 1978).

Acid volatile sulfide includes metastable iron sulfides like mackinawite and greigite and is termed monosulfide. The distribution in both

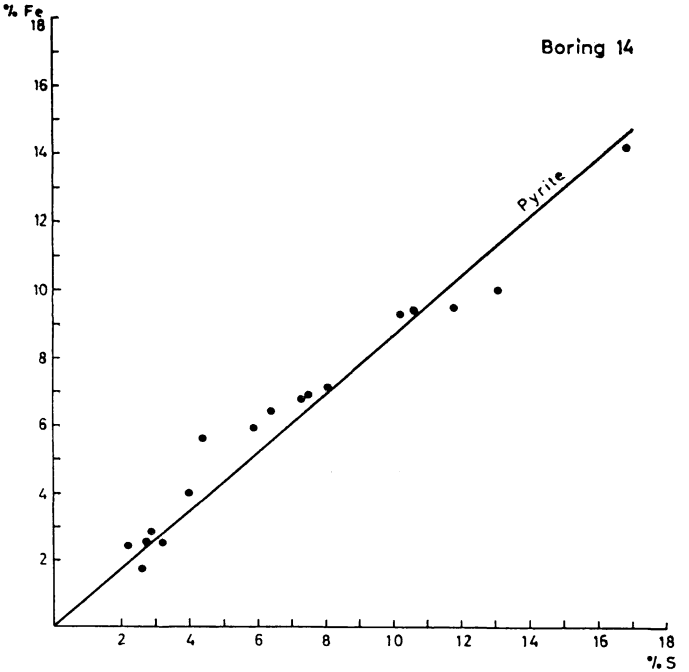

Fig. 3. The relation of total sulfur and aqua regia soluble iron (percent dry weight) in sediments of boring 14. Samples from the upper meter are excluded. The solid line corresponds to the Fe/S ratio in pyrite.

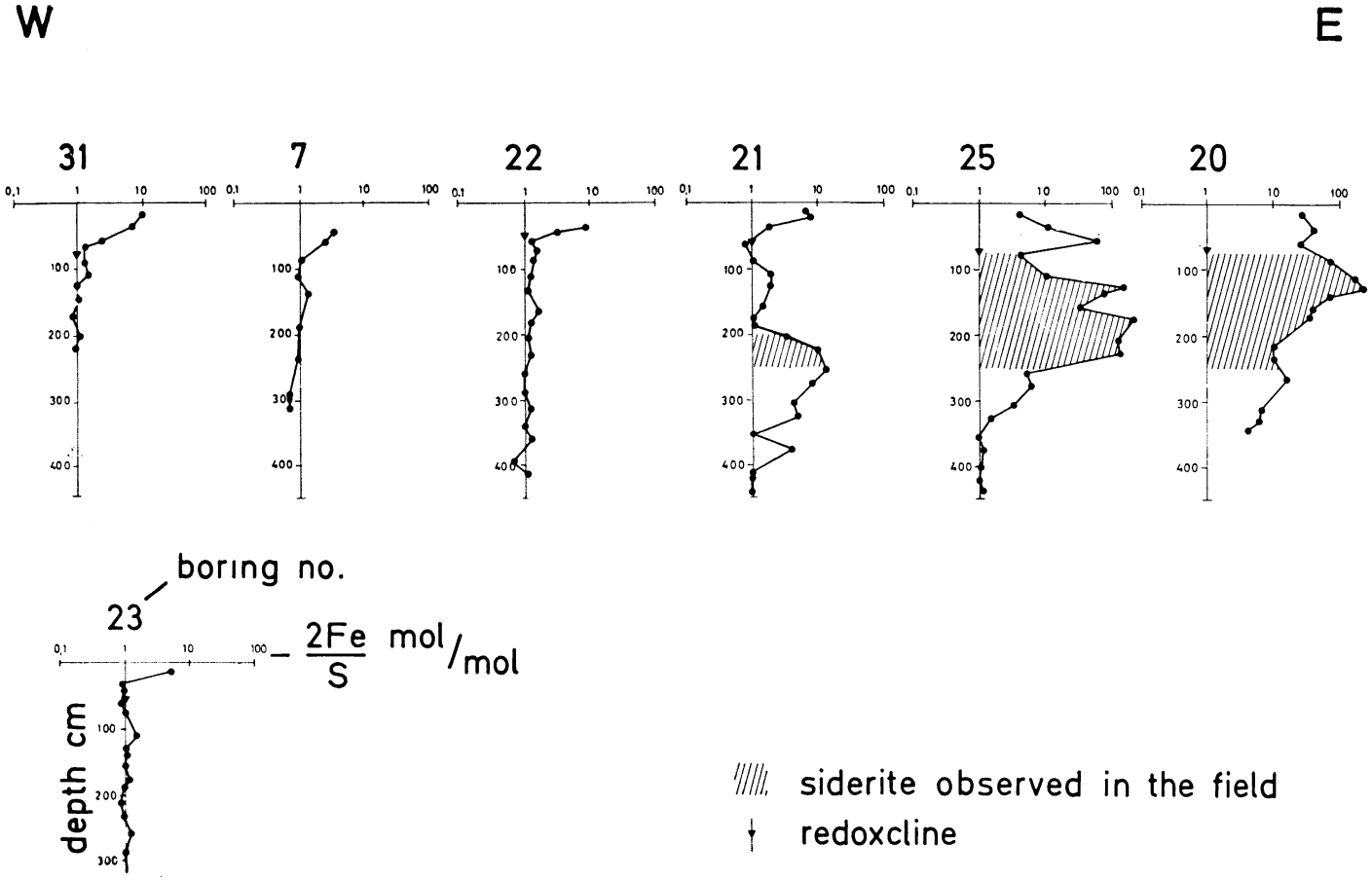

Fig. 4. Mole ratios of total sulfur and aqua regia soluble iron in sediments. A schematic east-west cross profile through Skjernå delta. Values of $2Fe/S = 1$ correspond to the ratio in pyrite.

borings 40 (fig. 5) and 41 (table 1) is the reverse of that usually encountered in marine sediments. In this case, traces of acid volatile sulfide are only found down to a depth of 4 m. The concentration of acid volatile sulfides usually decreases from the top of the sediment (Berner, 1970).

An example of measured phosphate contents in the sediments is shown in figure 6. In the pyritic sediments, the concentrations are low, less than 0.3 percent PO_4-P, which confirms the absence of the only identified phosphate mineral, vivianite, in these sediments.

In the eastern part of the peat basin where siderite and vivianite are found, the sediment chemistry is entirely different. Concentrations of iron are again very high and variable with depth (fig. 7). Values over 25 percent Fe have been measured in several cases in contrast to maxi-

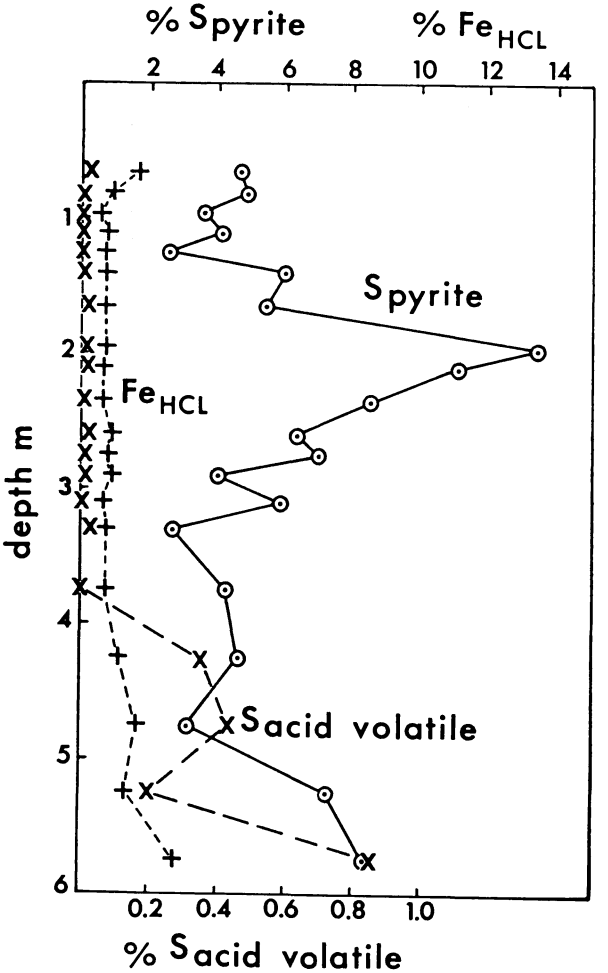

Fig. 5. Different forms of sulfur and iron in sediments of boring 40. All concentrations are expressed as percent dry weight. The redoxcline is situated at about 0.5 m depth.

TABLE 1

Forms of iron and sulfur in pyritic sediments of boring 41. Fe_{HCl} is "reactive iron", and P the degree of pyritization (see text).

Depth cm	Acid volatile S % dry wt	Fe_{HCl} % dry wt	S_{pyrite} % dry wt	P
65- 75	< 0.02	0.86	2.64	0.73
85- 95	< 0.02	1.20	4.32	0.76
105-115	< 0.02	1.53	2.58	0.60
120-130	< 0.02	1.31	1.91	0.56
135-145	< 0.02	1.39	3.76	0.70
170-180	< 0.02	1.12	4.55	0.78
185-195	0.02	0.78	6.29	0.88
205-215	0.02	0.53	2.04	0.77
222-232	< 0.02	0.59	2.16	0.76
243-253	0.02	0.90	7.61	0.88
260-270	< 0.02	0.85	5.99	0.86
285-295	< 0.02	0.79	4.23	0.82
310-320	< 0.02	0.58	4.54	0.87
335-345	< 0.02	0.63	7.41	0.91
360-370	< 0.02	0.70	8.74	0.92
385-395	0.05	0.72	6.26	0.88
420-430	0.37	1.73	6.03	0.75
455-465	0.08	1.07	5.95	0.83
480-490	0.02	0.88	6.92	0.87
505-515	0.02	0.85	8.48	0.89
530-540	< 0.02	0.73	8.12	0.91

mum values of 19 percent Fe in the pyritic area. Iron concentrations are on average also higher than in the pyritic area.

Results of carbonate and phosphate analyses are shown in table 2 and figure 6. Phosphate concentrations reach values as high as 0.9 percent PO_4-P, which is more than twice the maximum concentration encountered in the pyritic area. This endorses the field evidence where vivianite, with few exceptions, was always found together with siderite. If it is assumed that siderite and vivianite constitute the bulk of reactive iron in the sediments, a correlation between iron and the sum of carbonate and phosphate should be expected. While the correlation is acceptable (fig. 8), there is a very clear trend toward excess iron. Since the presence of monosulfides cannot explain this excess, and no other iron mineral was identified by X-ray diffraction, the most likely explanation for the excess iron is the assumption that X-ray amorphous iron oxides are present. If this is the case, it is conspicuous that the conversion of iron oxides to pyrite (fig. 3) is more complete than to siderite and vivianite.

Sulfur concentrations are very low in the sediments containing siderite. With only few exceptions, concentrations do not exceed a value of 1.0 percent S, whereas the large majority is well below 0.5 percent S. High Fe/S mole ratios, and in consequence high iron contents below the redoxcline, correspond very well with the observations of siderite in the field (fig. 4) and also with results of X-ray diffraction. The spatial separation of siderite and pyrite in the sediments is very clear, although small amounts of iron sulfide are found with siderite. Only in a few cases were siderite and pyrite identified in the same sample by X-ray diffraction. The

normal situation is, however, that these minerals occur in well-separated layers. In boring 25 for example, siderite is found in the upper 2.5 m of the sequence, while pyrite is found below this depth. Figure 9 combines the results of chemical analysis with mineral identification by X-ray diffraction for the same boring and shows that total concentrations of sulfur and iron reflect the presence of siderite or pyrite.

The distribution of siderite and pyrite may also be related to the environment in which the sediment has been deposited. While a 3-dimensional picture becomes extremely complicated due to the large spatial variations of different sediment types, a simplified picture can be constructed for the upper 2 m of the sediments. This corresponds to the layers just below the redoxcline.

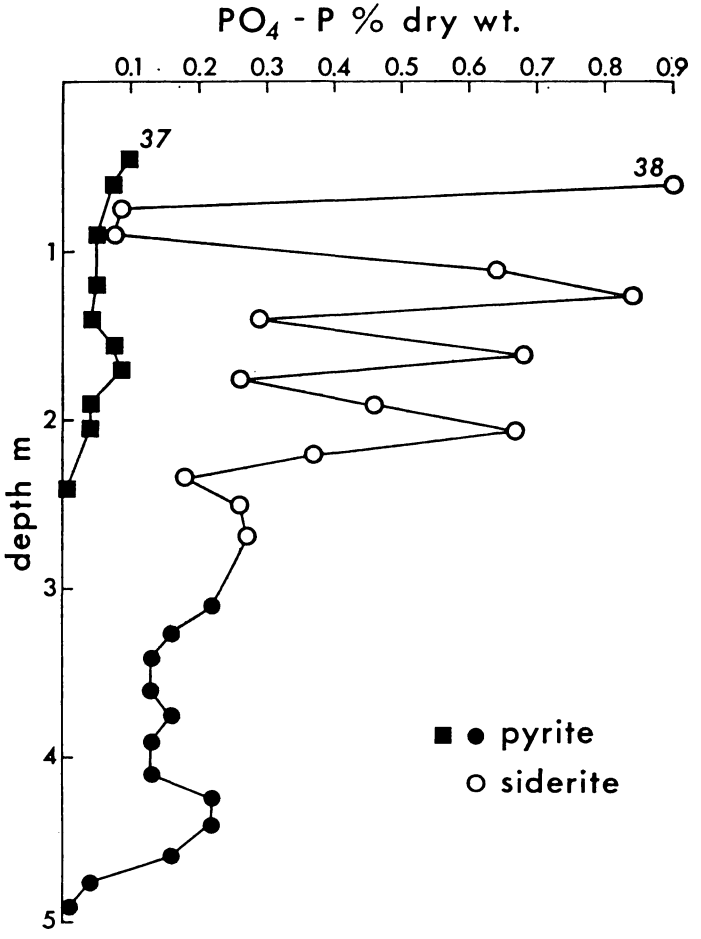

Fig. 6. Phosphate concentrations in sediments containing pyrite (filled symbols) or siderite (open symbols) in borings 37 and 38. Phosphate concentrations refer to HCl extractable phosphate.

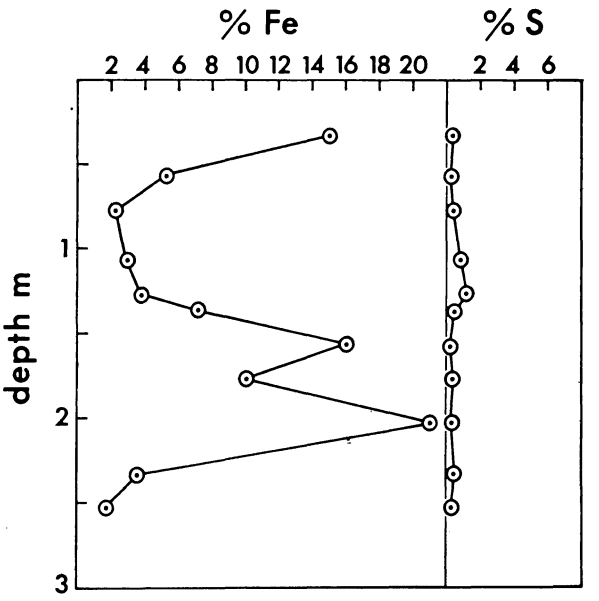

Fig. 7. Total sulfur and aqua regia soluble iron in the sideritic sediments of boring 29. The redoxcline is at 1 m depth.

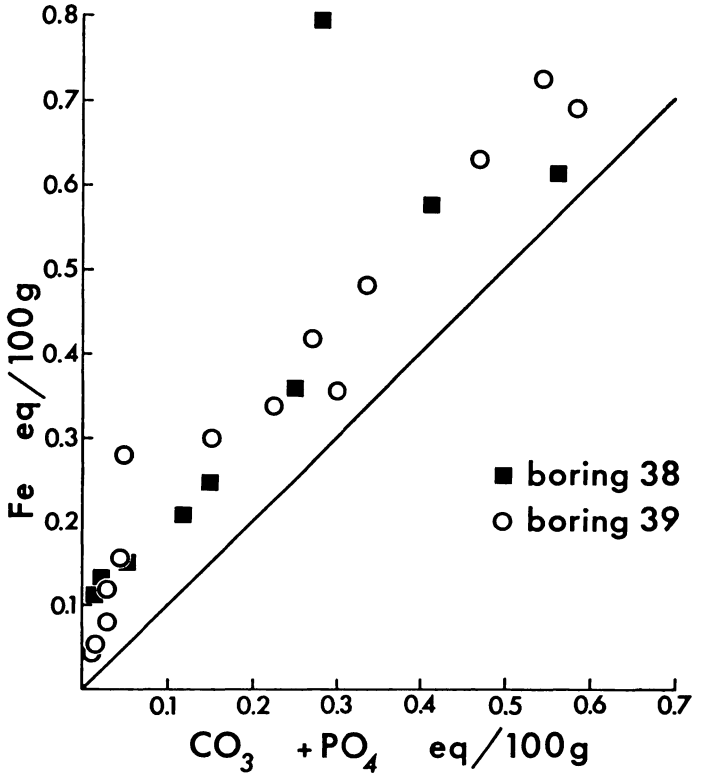

Fig. 8. "Reactive iron" (Fe_{HCl}) versus the sum of carbonate and phosphate in the sideritic sediments of borings 38 and 39. Concentrations are expressed as equivalents per 100 g dry weight. The solid line corresponds to the assumption that all "reactive iron" is present as siderite and vivianite.

TABLE 2

Chemical analysis of sideritic sediments from boring 39. Fe_{HCl} is "reactive iron", while phosphate refers to HCl extractable phosphate.

Depth cm	Acid volatile S % dry wt	Fe_{HCL} % dry wt	CO_3-C % dry wt	PO_4-P % dry wt
60- 70	< 0.02	1.39	0.06	0.06
90-100	0.02	3.31	0.09	0.14
125-135	0.06	7.83	0.13	0.28
175-185	< 0.02	17.56	2.57	0.43
200-210	< 0.02	13.37	1.51	0.88
230-240	< 0.02	20.23	2.94	0.59
260-270	0.02	11.68	1.12	0.84
290-300	0.04	4.35	0.16	0.20
325-335	< 0.02	19.28	2.99	0.88
360-370	0.06	9.43	0.83	0.88
390-400	0.03	8.41	0.40	0.89
425-435	< 0.02	9.89	1.31	0.86
460-470	< 0.02	2.20	0.15	0.07
490-500	< 0.02	1.17	0.04	0.03

For this purpose Halaburt (in preparation) constructed a distribution map for the upper 2 m, which shows the occurrence of brackish and freshwater sediments in the peat basin and is based on a general characterization of sediments (fig. 10). The distribution of pyrite and siderite as derived from chemical analysis of iron and sulfur, X-ray diffraction data, and field observations was superimposed on this map.

The results indicate (fig. 10) that the distribution of pyrite closely corresponds to the distribution of brackish water sediments, whereas

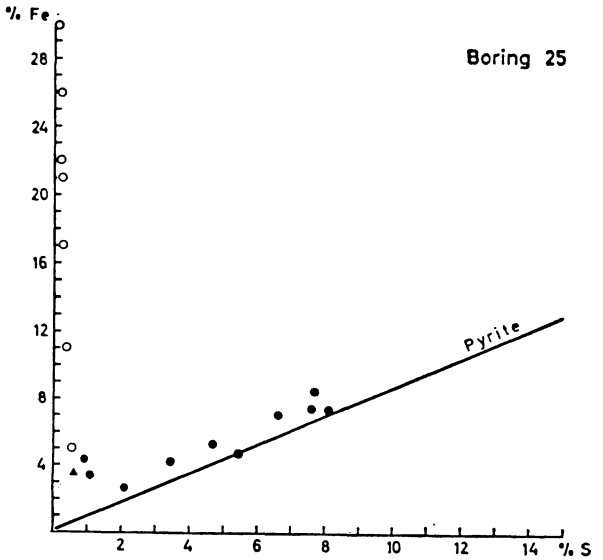

Fig. 9. Total sulfur and aqua regia soluble iron in sediments combined with results of X-ray diffraction. Open circles show that siderite was identified, filled circles pyrite, and the triangle neither pyrite nor siderite. The sediments of the upper meter have been excluded.

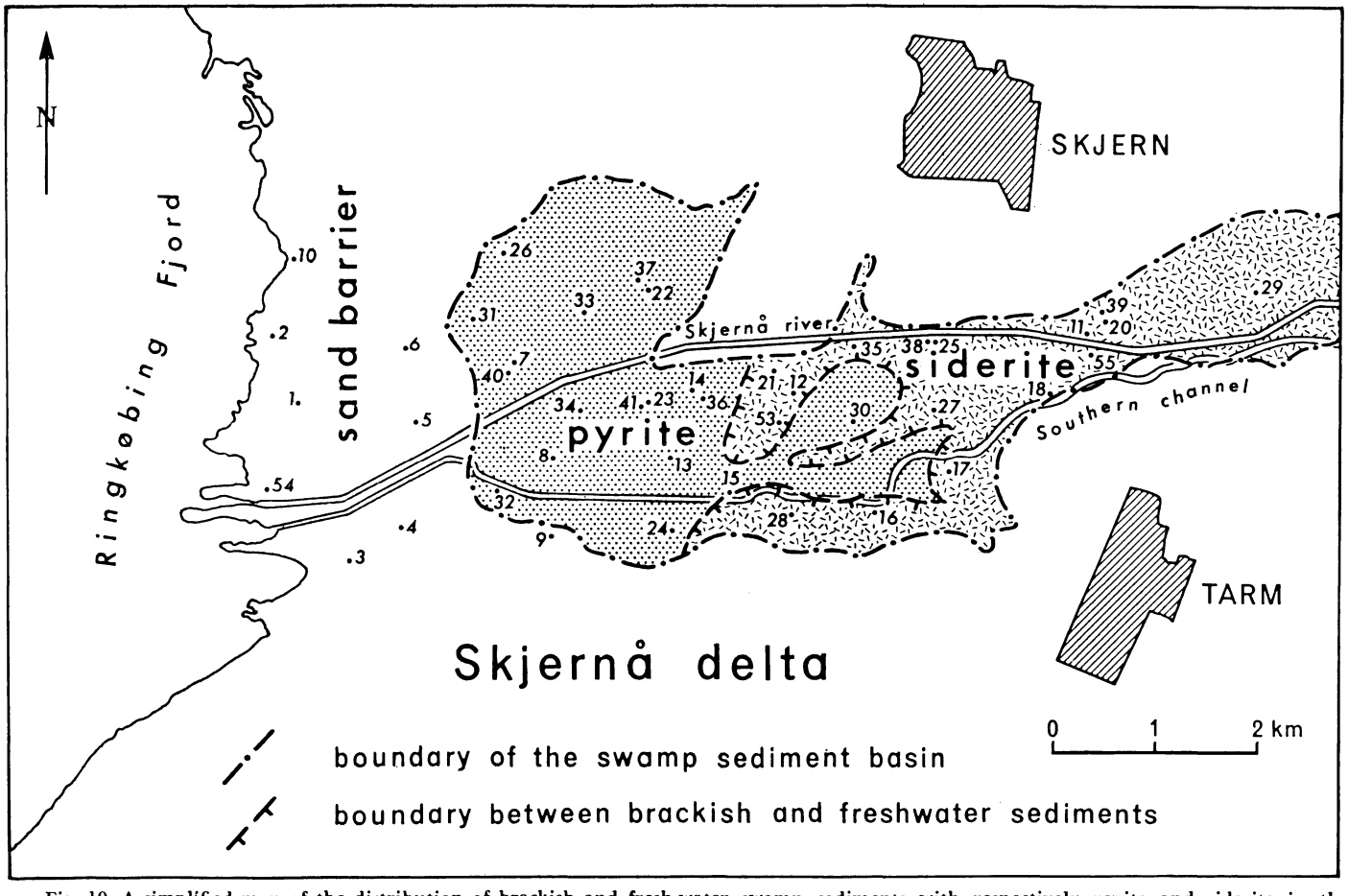

Fig. 10. A simplified map of the distribution of brackish and fresh water swamp sediments with respectively pyrite and siderite in the upper 2 m of the sequence in Skjernå delta. Numbers refer to borings. The division of brackish and freshwater sediments is from Halaburt (in preparation).

siderite is found only in freshwater sediments. It may therefore be concluded that the type of iron mineral formed apparently reflects the environment of deposition.

Pore water chemistry.—The occurrence of the different iron minerals in the various environments of the Skjernå-delta should be related to the pore water chemistry. In particular, this should be the case in the upper few meters of the sequence, while with increasing depth, the possibility of post-depositional changes of the pore water chemistry increases.

Reclamation of the area since the late sixties has modified the natural conditions and thereby complicates the interpretation of the pore water chemistry. Reclamation has resulted in a lowered watertable and has brought seawater influx to an end. The present-day lack of seawater influx is reflected by the decreasing upward trends of the chloride profiles (fig. 11). Tritium dating of the pore water (Postma, 1982) indicates, how-

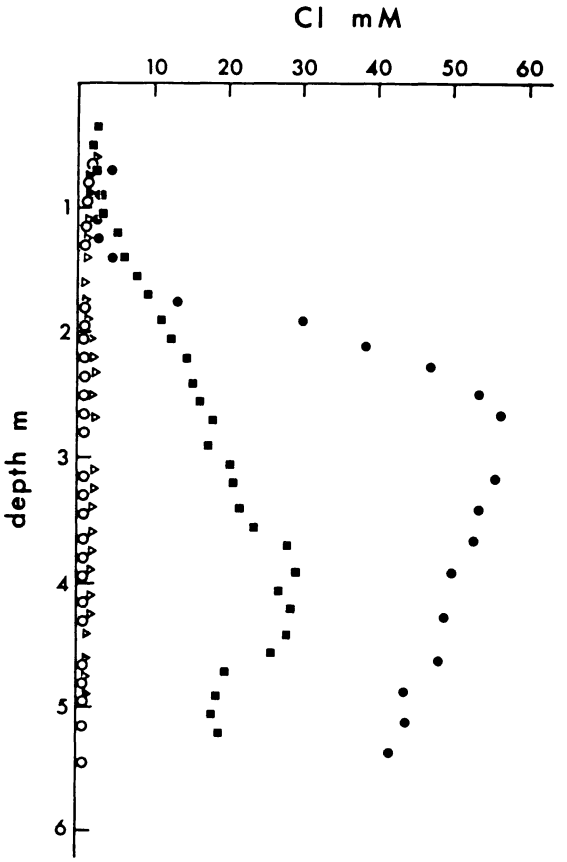

Fig. 11. Chloride profiles in pore waters. Open symbols: sideritic sediments, Closed symbols; pyritic sediments. ○ = boring 39, △ = boring 38, ■ = boring 36, and ● = boring 41.

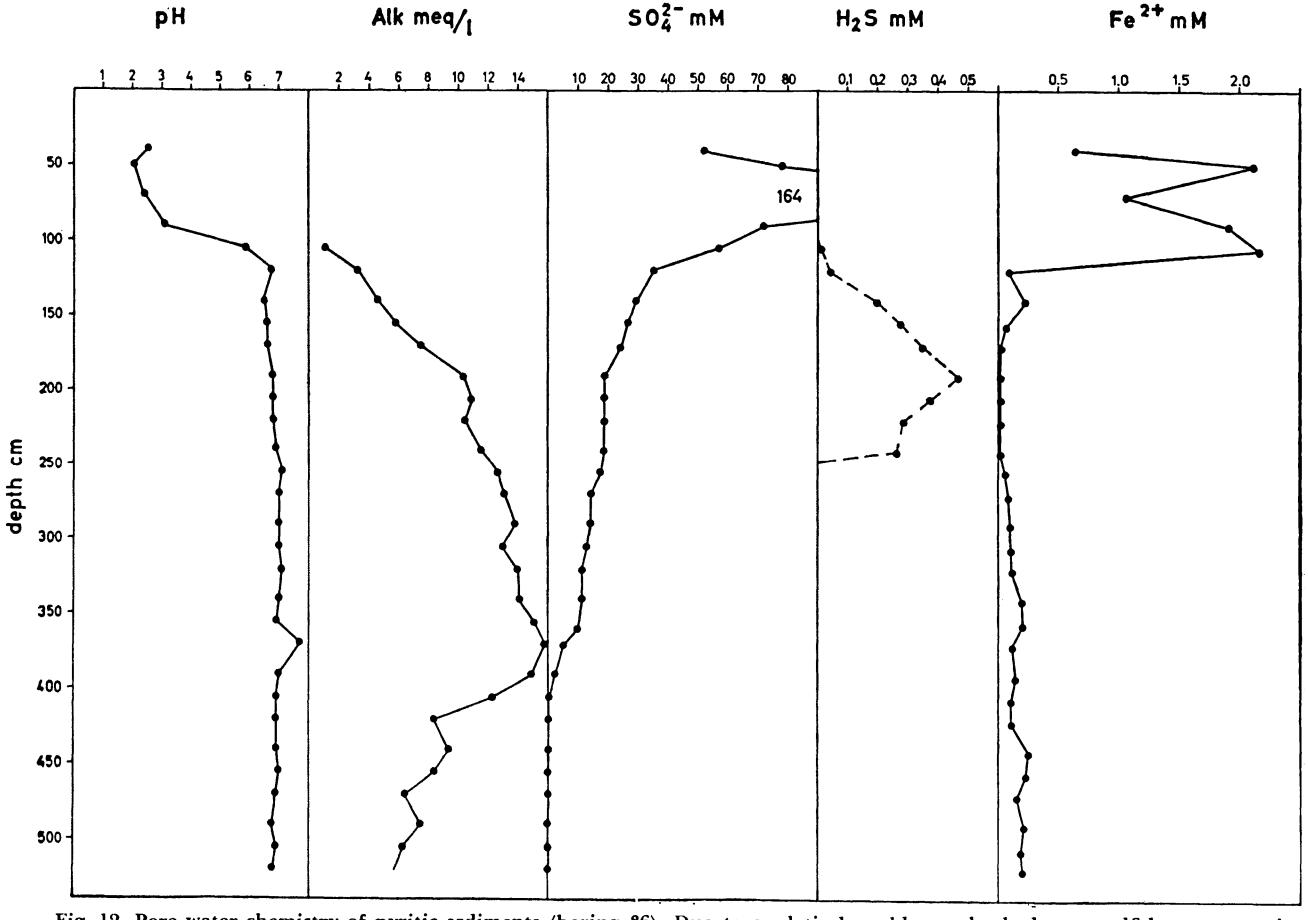

Fig. 12. Pore water chemistry of pyritic sediments (boring 36). Due to analytical problems, the hydrogen sulfide concentrations are minimum values.

ever, that virtually no infiltration occurs below the redoxcline. The decreasing upward trends of the chloride profiles are, therefore, mainly diffusion controlled, and the chloride concentration can still be used as a crude salinity indicator.

The chloride profiles (fig. 11), interpreted as such, confirm the relation between the occurrence of siderite and a freshwater environment, since borings 38 and 39 are the ones that contain siderite and at the same time show very low chloride levels. In boring 38, siderite is found only in the upper 2.5 m of the sequence, while at greater depths, only pyrite is found (see boring 25 nearby located, fig. 9). The other borings in which the pore water chemistry has been analyzed contained pyrite. These borings show much higher chloride concentrations, corresponding with the brackish origin of the sediments. It is believed that in the deeper parts of boring 38, a post-depositional change of pore water chemistry from brackish to freshwater has occurred.

Apart from salinity indicators such as Cl (and also Na and Mg), major differences in the pore water chemistry of borings with pyrite and siderite exist.

The pore water chemistry of the pyritic area is illustrated in boring 36 (fig. 12). At the top, in the oxidized zone, pyrite oxidation results in extremely low pH and very high sulfate and Fe^{2+} concentrations. Total Fe (< 0.45 μm) (not shown in fig. 12) is much higher than Fe^{2+} concentrations and reflects the presence of significant Fe^{3+} concentrations. The redoxcline coincides with a sharp increase in pH. In the reduced zone, sulfate concentrations decrease with depth and drop close to zero at a depth of about 4 m. Hydrogen sulfide is present in the pore water

TABLE 3

Pore water chemistry of pyrite containing sediments in boring 40.
$\log IAP_{FeS} = \log a_{Fe^{2+}} + \log a_{S^{2-}}$.

Depth cm	pH	SO_4 mM	ΣH_2S μM	Fe^{2+} mM	$-\log IAP_{FeS}$
60- 70	6.31	39.	< 5.	10.	
75- 85	6.74	21.	< 5.	0.75	
90-100	7.01	8.4	< 5.	0.20	
105-115	6.89	5.5	< 5.	0.065	
120-130	6.78	2.1	< 5.	0.020	
135-145	6.84	3.5	< 5.	0.013	
160-170	6.77	6.7	< 5.	0.009	
180-190	6.71	7.3	< 5.	0.029	
205-215	6.63	7.5	< 5.	0.025	
230-240	6.66	1.9	25.	0.014	17.25
255-265	6.61	0.76	26.	0.014	17.31
270-280	6.63	0.56	28.	0.013	17.33
285-295	6.64	0.57	20.	0.011	17.52
305-315	6.65	0.68	21.	0.011	17.49
325-335	6.73	0.46	10.	0.009	17.74
370-380	6.65	0.42	9.	0.007	18.04
420-430	6.59	0.40	10.	0.011	17.91
470-480	6.62	0.36	< 5.	0.009	
520-530	6.52	0.35	< 5.	0.12	
570-580	6.46	0.30	< 5.	0.38	

from the redoxcline to a depth of about 2.5 m. Ferrous iron concentrations drop rapidly below the redoxcline toward zero but remain measurable at a 0.25 to 0.01 mM level. It was observed that pore waters with high H_2S concentrations from boring 36 suddenly changed color after squeezing from clear to black because of acid volatile iron sulfide precipitation. This interfered with Fe^{2+} analysis which in this zone appears somewhat too low.

Hydrogen sulfide does not in all cases appear in the pore water just below the redoxcline, as in borings 36 and 37. In boring 40 (table 3), H_2S first appears at a depth of 2.3 m, where SO_4 is depleted to below 2 mM and H_2S reaches a value of only 0.028 mM, while in boring 41 it is completely absent.

Boring 38 (fig. 13) is used as an example for the pore water chemistry of the siderite dominated area. As should be expected, the pH in the oxidized zone is considerably higher than at the site of pyrite oxidation (Postma, 1982). The appearance of moderate sulfate concentrations above the redoxcline indicates the oxidation of small amounts of iron sulfide; in the reduced zone, however, sulfate concentrations quickly drop close to zero. Hydrogen sulfide is completely absent in the pore water. Furthermore, there is no increase in alkalinity with depth, but rather a decrease. Ferrous iron concentrations are dramatically high just below the redoxcline and decrease with depth. Fe^{2+} concentrations are generally much higher here than in the pyrite dominated area.

Saturation states of the pore water for different minerals have been calculated with a modified version of the computer program WATEQF (Plummer, Jones, and Truesdell, 1976). The thermodynamic data with quantitative significance for the calculations are the same as that of Postma (1981), while the rest is similar to the Truesdell and Jones (1974) compilation. Since ionic strengths of up to 0.3 are involved, activities are calculated from molar concentrations with the Davies equation rather than with the Debye-Hückel equation.

The results show that depth profiles of sideritic sediments (fig. 14) are dominated by supersaturation of up to one order of magnitude for siderite. The lower part of boring 38 shows, however, slight subsaturation for siderite, which coincides with the appearance of pyrite in this boring. On the other hand, boring 39 also displays slight subsaturation at its base, and this may well be a general feature. The large degree of supersaturation in the higher parts of both borings will be discussed in more detail below; this degree of supersaturation suggests however that siderite precipitation is an ongoing process.

The depth profiles in the pyritic area show two types of behavior. In the first type (fig. 15), strong subsaturation dominates. Just below the redoxcline, the downward transport of Fe^{2+} combined with the alkalinity increase, which is related to sulfate reduction, may result in a narrow zone of supersaturation for siderite.

In borings 36 and 37 (fig. 16), a different behavior is observed. Subsaturation for siderite is found here in the upper parts of the borings,

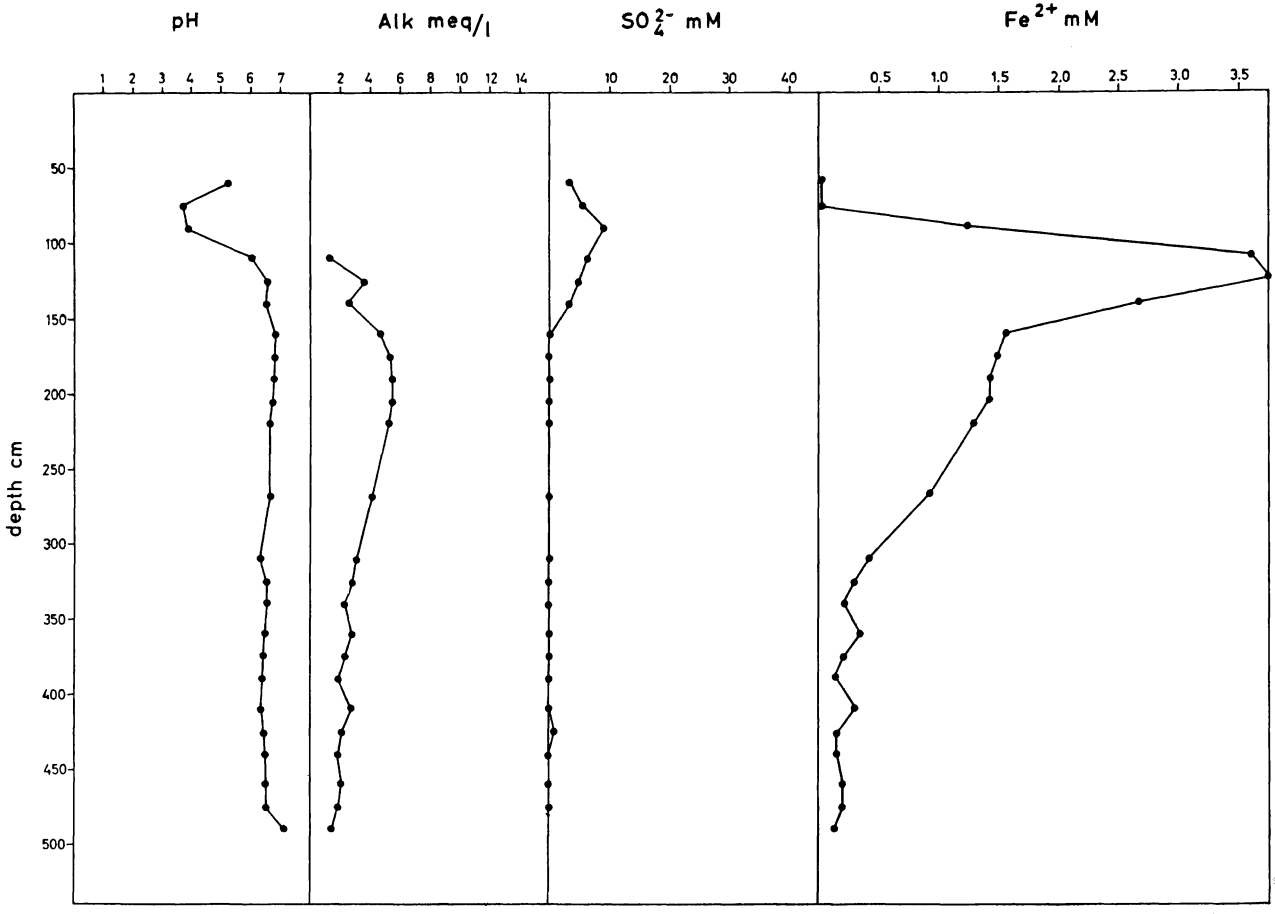

Fig. 13. Pore water chemistry of sideritic sediments (boring 38). Hydrogen sulfide is below detection limit (5 μM).

while with increasing depth when sulfate reduction is close to completion, equilibrium with siderite is approached.

Phosphate concentrations in pore waters are exemplified in table 4: boring 39 represents the freshwater area with siderite, and boring 40 the brackish pyritic area. Phosphate concentrations generally tend to increase with depth although they level off at the base. The most striking aspect is, however, that phosphate concentrations are far higher in the pyritic area than in the siderite area. When, on the other hand, the ion activity product for vivianite is calculated, the pattern is reversed. In boring 39,

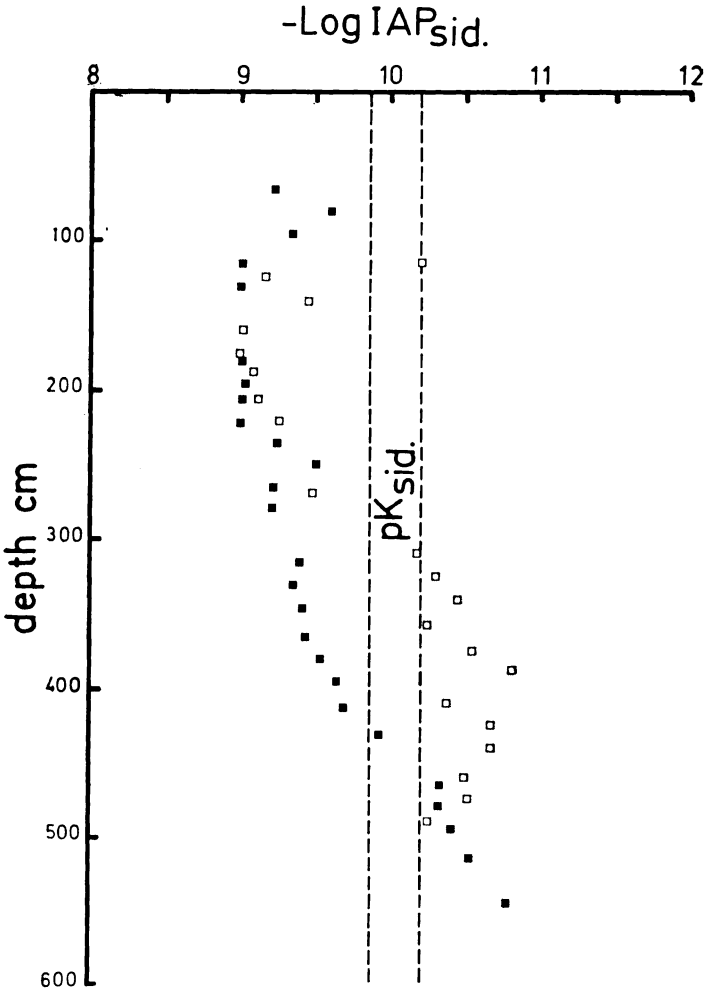

Fig. 14. The saturation state of the pore water for siderite in siderite containing sediments. log IAP_{sid} = log $a_{Fe^{2+}}$ + log $a_{CO_3^{2-}}$ and pK_{sid} = − log K_{sid}. Open squares = boring 38; closed squares = boring 39.

values for log IAP_{viv} (table 4) range mainly between −32 and −33 with a decreasing trend at the base. In the pyritic area (boring 40) the values are about five orders of magnitude lower. The low values for log IAP_{viv} encountered in boring 40 are, in spite of high phosphate concentration, mainly due to lower values of $a_{Fe^{2+}}$.

The calculated values for log IAP_{viv} can be compared with log K_{viv} = −36.0 measured by Nriagu (1972) or a value of −33.5 as determined by Tessenow (1974). Regardless of the chosen value, supersaturation dominates in boring 39. The high supersaturation for vivianite in the sideritic area together with the low phosphate concentrations are good arguments for ongoing vivianite precipitation. It is concluded that there

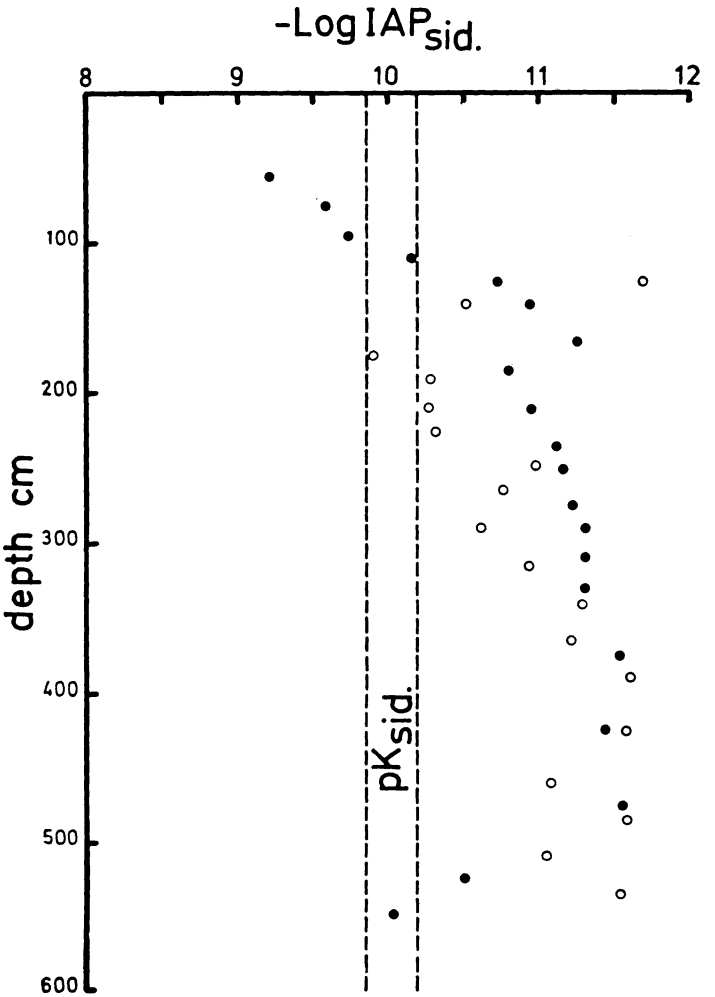

Fig. 15. The saturation state of the pore water for siderite in pyritic sediments. Open circles = boring 41; filled circles = boring 40.

is a good agreement between the saturation state of the pore water for vivianite and the presence or absence of the mineral in the sediments.

DISCUSSION

Berner (1964, 1971) theoretically demonstrated that siderite is only stable relative to pyrite at extremely low dissolved sulfide activities. This means that if sufficient hydrogen sulfide is produced by bacterial sulfate reduction, the precipitation of pyrite and other iron sulfides will never allow ferrous iron concentrations to reach a level whereby siderite becomes stable. Berner (1971) argued that, since seawater contains large amounts of sulfate, reducing conditions inevitably result in H_2S produc-

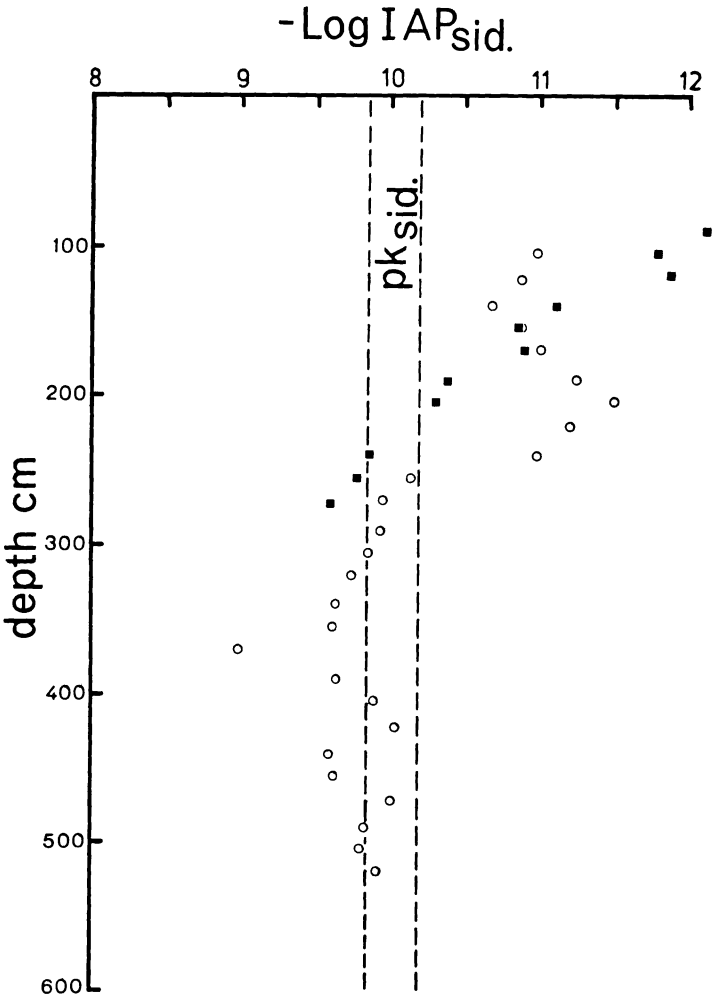

Fig. 16. The saturation state of the pore water for siderite in pyritic sediments. Circles = boring 36; squares = boring 37.

tion, and, as a result, siderite should not be stable in the marine environment.

The data from the Skjernå delta are consistent with these theoretical arguments. Siderite is dominantly found in freshwater sediments with pore waters of low chloride, no dissolved sulfide, and high ferrous iron concentrations. Pyrite on the other hand is found in brackish water sediments with pore waters containing much more chloride and low ferrous iron concentrations with the presence of dissolved sulfide in a number of cases. It is therefore concluded that a simple equilibrium model satisfactorily explains the overall distribution of siderite and pyrite in the sediments of the Skjernå delta.

Closer inspection of the data reveals several deviations from this simple model. In the siderite-containing sediments, for example, sulfate is found in the uppermost pore waters, although at much lower concentrations than in the pyritic borings. The major source for this sulfate is obviously oxidation of some iron sulfide or organic sulfur compounds. Freshwater will always contain some sulfate which, in the reduced zone, will inevitably result in the formation of some sulfide together with siderite. Organic sulfur may also serve as a sulfur source for pyrite formation. The low sulfur content of the freshwater sediments indicate, however, that organic sulfur could only yield small amounts of pyrite.

TABLE 4

Phosphate in pore waters of the sideritic boring 39 and the pyritic boring 40. $\log IAP_{vlv} = 3\log a_{Fe^{2+}} + 2\log a_{PO_4^{3-}}$.

Boring 39			Boring 40		
Depth cm	PO_4 μM	$-\log IAP_{vlv}$	Depth cm	PO_4 μM	$-\log IAP_{vlv}$
60- 70	16.	32 6	60- 70	5.	34.2
75- 85	7.	34.1	75- 85	3.	35.9
90-100	10.	33.4	90-100	9.	35.4
110-120	11.	33.0	105-115	16.	36.5
125-135	13.	32.7	120-130	57.	37.2
175-185	22.	32.4	135-145	86.	37.3
190-200	17.	32.6	160-170	97.	38.1
200-210	19.	32.3	180-190	83.	36.9
215-225	34.	32.0	205-215	84.	37.3
230-240	41.	32.2	230-240	154.	37.3
245-255	21.	33.2	255-265	191.	37.3
260-270	25.	32.8	270-280	211.	37.3
275-280	21.	32.8	285-295	211.	37.5
310-320	53.	32.1	305-315	184.	37.6
325-335	58.	31.8	325-335	200.	37.6
360-370	53.	32.0	370-380	200.	38.1
375-385	65.	32.0	420-430	200.	37.8
390-400	58.	32.3	470-480	158.	38.2
410-420	33.	32.9	520-530	137.	35.2
425-435	46.	33.0	570-580	104.	34.2
460-470	40.	34.0			
475-485	38.	34.2			
490-500	38.	34.3			
510-520	33.	35.0			
540-550	22.	35.8			

The borings of the pyritic area are, according to the simple model, expected to show subsaturation for siderite, as is the case in two of the borings (fig. 15). However, in the other two borings (fig. 16), the IAP_{sid} increases with depth, until equilibrium or slight supersaturation for siderite is reached. The increase of IAP_{sid} is partly related to the alkalinity increase induced by sulfate reduction and partly to the slightly higher ferrous iron concentrations below the zone where H_2S is found in the pore water. Martens, Berner, and Rosenfeld (1978) reported a somewhat similar situation from Long Island Sound and found that dissolved iron concentrations increase markedly below the zone where sulfate reduction is complete. Ion activity products for siderite are not given in this paper but could be expected to exceed the solubility product of siderite.

Increasing ferrous iron concentrations below the zone where sulfate reduction is complete might well represent a general model along which "secondary" siderite could form in marine sediments. An additional constraint is, however, that Fe/Ca ratios of the pore water should be high enough to stabilize siderite over calcite (Berner, 1971).

No evidence for such "secondary" siderite has been found in the Skjernå delta sediments. The question is, however, whether it could be of quantitative significance, since the content of reactive iron (Fe_{HCl}) which includes siderite-iron is small (fig. 5 and table 1).

Siderite formation.—In the siderite-containing sediments, the pore water is supersaturated with siderite by up to one magnitude. Such large supersaturations for siderite have been found in a number of studies (Emerson, 1976; Bricker and Troup, 1975; Postma, 1981) and are apparently a general feature. Postma (1981) discussed possible analytical artifacts as well as effects of organic complexing and concluded that these factors hardly represent a general explanation for these supersaturations.

SEM micrographs showed that the siderite crystals in the sediments have an extremely small crystal size with a tendency to overgrowth. This seems to be at terms with precipitation from highly supersaturated solutions. A matter of some concern, however, is the application of solubility products to such fine-grain sizes as those found here for both siderite and vivianite. For crystal sizes of less than 1 micron, the solubility increases significantly with decreasing grain size.

Theoretically, the problem can be approached with the Kelvin equation (Adamson, 1976). Application of the Kelvin equation requires, however, the knowledge of the surface free energy of siderite, and this value was not found in the literature. Alternatively, a parallel can be drawn to the case of calcite.

Chave and Schmalz (1966) reported that the solubility of calcite for particles between 0.1 and 0.01 μ increases by almost one order of magnitude. Additionally, the solubility for a mixture of crystals with different sizes is known to be determined by the smallest crystal size present (Enüstün and Turkevich, 1960).

SEM work on the siderite occurring in the Skjernå delta sediments showed the presence of crystal sizes of less than 0.1 μ. The smallest crystal

size is thus within the range where grain-size effects on the solubility become important. Although this effect cannot be quantified at present, we may note that the observed supersaturations for siderite of up to one order of magnitude (fig. 14) are in the same range as what was found for calcite particles between 0.1 and 0.01 μ by Chave and Schmalz (1966). The grain size effect on the solubility of siderite thereby appears to be a possible explanation for the high degrees of supersaturation found in this and other studies.

The fine siderite crystallites are, of course, unstable in comparison with larger crystals and are only likely to persist as long as high values for IAP_{sid} are maintained. This poses the question of by which process siderite actually is formed. Postma (1977, 1981) proposed 2 mechanisms for siderite formation: (A) the replacement of $CaCO_3$, and (B) the reduction of ferric oxyhydroxides. The replacement of $CaCO_3$ is highly unlikely at the present locality since the deposits close to the surface in this area contain little or no $CaCO_3$, while Skjernå delta sediments are also practically free of $CaCO_3$. The reduction of ferric oxyhydroxides by organic matter provides both a source of Fe^{2+} and of carbonate for siderite formation as is illustrated by an overall reaction of the type

$$4FeOOH + CH_2O + 3H_2CO_3 \rightarrow 4FeCO_3 + 6H_2O$$

In this reaction, CH_2O represents organic matter, and the stoichiometry is, of course, only approximate. Still the reaction illustrates that the base producing effect of FeOOH reduction more than balances the acid production from organic matter's oxidation as is reflected by the consumption of H_2CO_3. To establish that a reaction of this kind is at all possible, a pilot experiment was carried out in which fine-grained goethite was mixed with fresh water sewage sludge, freed of $CaCO_3$ by acid washing. The initial pH was adjusted to 6 with NH_4OH, and the mixture was stored in a sealed jar in the dark at room temperature. After about 3 weeks, siderite became visible, and a check by X-ray diffraction after 2 months showed broad reflections corresponding to siderite. Further work on experimental siderite formation is planned. So far, the experiment indicates that siderite formation through the reduction of ferric oxyhydroxides by organic matter is a feasible process.

Vivianite formation.—The conditions in which vivianite forms are in many respects similar to those for siderite. As in the case of siderite, it is the Fe^{2+} activity, rather than the phosphate concentration, that actually determines whether or not saturation for vivianite is attained (table 4). Since $a_{Fe^{2+}}$ is again controlled by the sulfide production, the constraints on the formation of vivianite are similar to those for siderite. This is consistent with the common association of vivianite and siderite (Bricker and Troup, 1975; Anthony, 1977; Postma, 1977). The most favorable conditions for vivianite formation are therefore anoxic freshwater environments as in this case, as well as in many other freshwater sediments (Rosenqvist, 1970; Tessenow, 1973; Nriagu and Dell, 1974; Mothersill, 1975; Anthony, 1977; Postma, 1977).

Under marine conditions, however, formation should be possible below the level where sulfate reduction is complete, as indicated by calculated saturation states (Martens, Berner, and Rosenfeld, 1978). To the author's knowledge, however, vivianite has never been found in recent marine sediments. The closest report is that of Bricker and Troup (1975), who found vivianite in the northern (freshwater) part of Chesapeake Bay sediments. Unfortunately, these authors do not report the salinity of the pore waters for the sediments in which vivianite was found. Due to the conspicuous appearance of vivianite in partly oxidized form, it is unlikely that vivianite would be missed during routine sediment examination.

Pyrite formation.—Pyrite formation starts with bacterial sulfate reduction. The produced H_2S reacts with fine-grained Fe(III) compounds, precipitating iron monosulfides, such as mackinawite and greigite (Berner, 1970).

These monosulfides are metastable relative to pyrite (Berner, 1967). Monosulfides, therefore, usually disappear with increasing sediment depth. The transformation of monosulfide to pyrite takes place by sulfur addition rather than iron subtraction (Berner, 1970; Sweeney and Kaplan, 1973). The monosulfides react with elemental sulfur and dissolved H_2S producing pyrite. This reaction is rate-limiting (Rickard, 1974, 1975) in the process of pyrite formation. Howarth (1979) recently presented evidence for faster pyrite formation in salt marsh sediments, without intermediate monosulfide formation. Howarth (1979) argued that the pore waters of these marsh sediments are subsaturated for monosulfides but supersaturated for pyrite which allows direct pyrite precipitation.

For an evaluation of present day pyrite formation in Skjernå delta sediments, it should be born in mind that the present conditions are not necessarily identical to those before reclamation. Major results of reclamation are both the hindrance of seawater influx and the intensification of oxidation. It is thus observed that sulfate profiles (fig. 12) are inverse to chloride profiles (fig. 11), and the contribution of seawater sulfate to the present sulfate content of the pore water appears to be negligible. Instead, the sulfate profiles are generated by present-day pyrite oxidation in the top layers.

The presence of hydrogen sulfides in the pore waters demonstrates ongoing sulfate reduction and sulfate profiles are therefore not solely transport-controlled. Ongoing sulfate reduction is also illustrated by the strong alkalinity increase coupled to decreasing sulfate concentrations (fig. 12) (Berner, Scott, and Thomlinson, 1970).

Since hydrogen sulfide is limited to certain levels and is even absent in one boring, precipitation of iron sulfide can be inferred. Sediment analyses (fig. 5 and table 1) show, however, that monosulfides are not present in the top of the reduced zone where they are usually found in marine sediments. Absence of monosulfide occurs occasionally in marshes and swamps (van Breemen, ms; Howarth, 1979; Howarth and Teal, 1979), thus strongly favoring the mechanism of pyrite formation proposed

by Howarth (1979). Howarth's argument, subsaturation for monosulfides but supersaturation for pyrite, can be tested by calculating the ion activity products from the pore water composition. In boring 41, dissolved hydrogen sulfide was below detection limit, and at the observed pH, the values for log IAP_{FeS} (= log $a_{Fe^{2+}}$ + log $a_{S^{2-}}$) are less than −17.

For boring 40 (table 3), calculated values for log IAP_{FeS} range from −17.25 to −18.04. Berner (1967) gives amorphous FeS a value of log K = −16.9 and mackinawite log K = −17.6. The values found here are thus very close to equilibrium with mackinawite. However, precipitation of mackinawite cannot be very significant as little or no monosulfide is found at these depths. Thus the evidence for pyrite formation according to the Howarth mechanism is somewhat ambiguous, although the lack of monosulfide in the top of the reduced zone and the absence of hydrogen sulfide in parts of the borings where sulfate depletion continues can be considered as indirect evidence.

Monosulfides are in fact found at the base of both boring 40 and 41, in both cases at a depth of from 4 m downward, and at this level sulfate reduction is complete. A possible explanation could be diffusion of sulfate into the peat from the underlying sandy deposits, followed by sulfate reduction and monosulfide precipitation. This has been observed at another locality (unpublished data) but appears to be of no importance in these borings at the present. Alternatively, an origin related to ancient salinity changes as proposed by Berner (1974) may be possible.

Two other borings from the pyritic area, borings 36 (fig. 12) and 37, show much higher hydrogen sulfide concentrations in the pore waters. In boring 36, where the calculated values for log IAP_{FeS} range from −15.65 to −16.98, monosulfides should precipitate. In fact, monosulfide precipitation was observed after pore water squeezing, and this suggests that monosulfide precipitation in the sediments is transport-controlled. Such behavior can be explained by the presence of microniches in the sediments where sulfate reduction occurs. The existence of microniches as centers for sulfate reduction has been documented by Jørgensen (1977a).

Unfortunately there are no analyses of monosulfides in the sediments available from these borings. It seems reasonable to suppose though that pyrite formation occurs in these borings according to the traditional scheme with monosulfides as an intermediate.

Pyrite concentrations in Skjernå delta sediments are unusually high, and the degree of pyritization here is also much higher than in most marine sediments.

The high pyrite concentrations, expressed as percent S dry weight, are partly due to the limited dilution by inorganic clastic material. Sulfur concentrations in boring 23 (fig. 2) range from 0.94 to 12 percent total S dry weight, which corresponds to about 0.15 to 1.2 mmol S/cm^3. For comparison, Jørgensen (1977b) found up to 0.4 mmol S/cm^3 in coastal marine sediments from Limfjorden. Pyrite concentrations in Skjernå delta sediments are thus also per volume significantly higher. The main difference between the two environments is the degree of pyritization.

Whilst in Skjernå delta a degree of pyritization of up to 0.95 is found, maximum values in Limfjorden are about 0.5 (Jørgensen, 1978). If all reactive iron in Limfjorden was converted to pyrite, the pyrite content of the sediments in the two environments would be more or less comparable.

Nedwell and Abram (1978) explained the high degree of pyritization in some salt marsh sediments and low values in others, in terms of differences in H_2S loss from the sediment. Jørgensen (1977b) found that in Limfjorden only 10 percent of the produced H_2S is fixed as iron sulfide in the sediment, while the remainder is lost by diffusion and reoxidation. The rate of H_2S fixation by iron sulfide precipitation depends to a large extent on the reactivity of the available iron oxides (for example, grain size, crystallinity) and the H_2S concentration. If less H_2S was lost from the sediment, more iron sulfide precipitation is to be expected, and the result should be a higher degree of pyritization. It might well be worth while to consider that, in the absence of tidal flushing, marshes and swamps behave more like a closed system for H_2S than the surface layer of a marine sediment, due to less resuspension and burrowing. This would be a reasonable explanation for the sometimes observed high degree of pyritization in marshes and swamps (van Breemen, ms; Nedwell and Abrams, 1978; and this study).

Sources of iron and sulfur.—The accumulation of high concentrations of pyrite and siderite in Skjernå delta sediments calls for some comments on the origin of the iron and sulfur. The association of pyrite with brackish water sediments explains the source of sulfur. The sulfate supply from seawater has apparently been a limiting factor for the formation of pyrite.

The contribution of organic sulfur as a source for pyrite sulfur appears to be quite insignificant. This is shown by the low sulfur content of sideritic sediments (< 1 percent S dry weight) even though organic carbon contents of more than 25 percent C dry weight have been measured. Furthermore, the good correlation between Fe and S in pyritic sediments (fig. 3) does not suggest the presence of large amounts of organic sulfur. Jørgensen (1977b) measured organic sulfur contents from 0.3 percent S dry weight in eelgrass, which is perhaps most comparable to the organic matter found here, to 1 to 2 percent S dry weight in plankton. Even if the sediments consisted exclusively of organic matter, the organic sulfur contribution would thus be small compared to the measured concentrations in the sediments.

The iron distribution in the sediments of the delta is more even than that of sulfur, although the highest iron concentrations are definitely found in the eastern parts. This indicates that the iron transport by the Skjernå river has been the dominant iron source for the Skjernå delta sediments. Investigations during 1976 and 1977 (J. Jacobsen, personal commun.) have shown that the total iron transport by the Skjernå river is about 2300 tons per yr and occurs almost exclusively in suspension and by bottom sediment transport. It was estimated that, about 1600 tons Fe per yr (corresponding to about 2 mg/l Fe) can be considered as being

the natural background value, while the remainder is due to pollution and drainage. Before reclamation of the Skjernå delta, a significant part of the iron transported by the river must have been deposited by sedimentation in the swamp sediments. A quantitative estimate of the mean annual iron deposition rate is unfeasible due to uncertain sediment deposition rates, but rough calculations indicate that the accumulated iron in the sediments represents only a minor part of the total iron transport in post-glacial times.

CONCLUSIONS

The distribution of siderite and vivianite on the one hand and pyrite on the other is, in Skjernå delta swamp sediments, related to respectively fresh and brackish water environments. This distribution is satisfactorily explained by a simple equilibrium model and is supported by the pore water chemistry.

Nevertheless, siderite cannot be considered as a safe paleo-environmental freshwater indicator, since siderite in minor amounts may also form in brackish or marine environments below the zone where sulfate reduction is complete if sufficient remaining iron is available.

It is proposed that the reduction of ferric oxyhydroxides by organic matter in the absence of sulfide production results in the formation of siderite.

The formation of pyrite appears in some cases to occur by direct pyrite precipitation as proposed by Howarth (1979), without intermediate monosulfide formation.

ACKNOWLEDGMENTS

Part of this work was carried out while the author was at the Geochemical Department of the Geological Survey of Denmark, and the help and support of the staff is gratefully acknowledged. Special thanks are due to Ellen Zimmer Hansen and Lotte Nielsen for assistance during fieldwork. Analytical work by Birgit Damgaard is also acknowledged. I am especially obliged to David Rickard and Jens Jacobsen for stimulating discussions and reviews. This work has been supported by a grant from the Danish Natural Science Research Council.

REFERENCES

Adamson, A. W., 1976, Physical chemistry of surfaces, 3d ed.: New York, John Wiley & Sons, 698 p.

Anthony, R. S., 1977, Iron-rich rhythmically laminated sediments in Lake of the Clouds, northeastern Minnesota: Limnology Oceanography, v. 22, p. 45-54.

Berner, R. A., 1964, Stability fields of iron minerals in anaerobic marine sediments: Jour. Geology, v. 72, p. 826-834.

———— 1967, Thermodynamic stability of sedimentary iron sulfides: Am. Jour. Sci., v. 265, p. 773-785.

———— 1970, Sedimentary pyrite formation: Am. Jour. Sci., v. 268, p. 1-23.

———— 1971, Principles of Chemical Sedimentology: New York, McGraw-Hill, 240 p.

———— 1974, Iron sulfides in pleistocene deep Black Sea sediments and their paleo-oceanographic significance, *in* Degens, E. T., and Ross, D. A., eds., The Black Sea — geology, chemistry, and biology: Am. Assoc. Petroleum Geologists Mem. 20, p. 524-531.

Berner, R. A., Baldwin, T., and Holdren, G. R., Jr., 1979, Authigenic iron sulfides as paleosalinity indicators: Jour. Sed. Petrology, v. 49, p. 1345-1350.

Berner, R. A., Scott, M. R., and Thomlinson, C., 1970, Carbonate alkalinity in the pore waters of anoxic marine sediments: Limnology Oceanography, v. 15, p. 544-549.

Bricker, O. P., and Troup, B. N., 1975, Sediment-water exchange in Chesapeake Bay, *in* Cronin, L. E., ed., Estuarine Research, v. 1: New York, Academic Press, p. 3-27.

Chave, K. E., and Schmalz, R. F., 1966, Carbonate-seawater reactions: Geochim. et Cosmochim. Acta, v. 30, p. 1037-1048.

Curtis, C. D., 1967, Diagenetic iron minerals in some British Carboniferous sediments: Geochim. et Cosmochim. Acta, v. 31, p. 2109-2123.

Emerson, S., 1976, Early diagenesis in anaerobic lake sediments: chemical equilibria in interstitial waters: Geochim. et Cosmochim. Acta, v. 40, p. 925-934.

Enüstün, B. V., and Turkevich, J., 1960, Solubility of fine particles of strontium sulfate: Am. Chem. Soc. Jour., v. 82, p. 4502-4509.

Faye, G. H., Manning, P. G., and Nickel, E. H., 1968, The polarized optical absorption spectra of tourmaline, cordierite, chloritoid and vivianite: ferrous-ferric electronic interaction as a source of pleochroism: Am. Mineralogist, v. 53, p. 1174-1201.

Garrels, R. M., and Christ, C. L., 1965, Solutions, minerals and equilibria: New York, Harper & Row, 450 p.

Goldhaber, M. B., Aller, R. C., Cochran, J. K., Rosenfeld, J., Martens, C. S., and Berner, R. A., 1977, Sulfate reduction, diffusion, and bioturbation in Long Island Sound sediments: report of the FOAM group: Am. Jour. Sci., v. 277, p. 193-237.

Goldhaber, M. B., and Kaplan, I. R., 1974, The sulfur cycle, *in* Goldberg, E. D., ed., The Sea, v. 5, Marine Chemistry: New York, John Wiley & Sons, p. 569-655.

Harwood, J. E., van Steenderen, R. A., and Kühn, A. L., 1969, A rapid method for orthophosphate analysis at high concentrations in water: Water Research, v. 3, p. 417-423.

Howarth, R. W., 1979, Pyrite: its rapid formation in a salt marsh and its importance in ecosystem metabolism: Science, v. 203, p. 49-51.

Howarth, R. W., and Teal, J. M., 1979, Sulfate reduction in a New England salt marsh: Limnology Oceanography, v. 24, p. 999-1013.

Jørgensen, B. B., 1977a, Bacterial sulfate reduction within reduced microniches of oxidized marine sediments: Marine Biology, v. 41, p. 7-17.

———— 1977b, The sulfur cycle of a coastal marine sediment (Limfjorden, Denmark): Limnology Oceanography, v. 22, p. 814-832.

———— 1978, A comparison of methods for the quantification of bacterial sulfate reduction in coastal marine sediments: III Estimation from chemical and bacteriological field data: Geomicrobiol. Jour., v. 1, p. 49-64.

Kaplan, I. R., Emery, K. O., and Rittenberg, S. C., 1963, The distribution and isotopic abundance of sulphur in recent marine sediments off southern California: Geochim. et Cosmochim. Acta, v. 27, p. 297-331.

Love, L. G., 1971, Early diagenetic polyframboidal pyrite, primary and redeposited from the Wenlockian Denbigh Grit Group, Conway, North Wales, U.K.: Jour. Sed. Petrology, v. 41, p. 1038-1044.

Love, L. G., and Murray, J. W., 1963, Biogenic pyrite in recent sediments of Christchurch harbour, England: Am. Jour. Sci., v. 261, p. 433-448.

Martens, C. S., Berner, R. A., and Rosenfeld, J., 1978, Interstitial water chemistry of anoxic Long Island Sound sediments: II-Nutrient regeneration and phosphate removal: Limnology Oceanography, v. 23, p. 605-617.

McCammon, C. A., and Burns, R. G., 1980, The oxidation mechanism of vivianite as studied by Mössbauer spectroscopy: Am. Mineralogist, v. 65, p. 361-366.

Mothersill, J. S., 1975, The formation of vivianite in the sediments of Lake Victoria: Internat. Cong. Sedimentology, 9th, Nice, v. 2, p. 93-101.

Nedwell, D. B., and Abram, J. W., 1978, Bacterial sulphate reduction in relation to sulphur geochemistry in two contrasting areas of salt marsh sediment: Estuarine Coastal Marine Sci., v. 6, p. 341-351.

Nriagu, J. O., 1972, Stability of vivianite and ion-pair formation in the system $Fe_3(PO_4)_2$–H_3PO_4–H_2O: Geochim. et Cosmochim. Acta, v. 36, p. 459-470.

Nriagu, J. O., and Dell, C. I., 1974, Diagenetic formation of iron phosphates in recent lake sediments: Am. Mineralogist, v. 59, p. 934-946.

Pearson, M. J., 1979, Geochemistry of the Hepworth Carboniferous sediment sequence and origin of the diagenetic iron minerals and concretions: Geochim. et Cosmochim. Acta, v. 43, p. 927-941.

Plummer, L. N., Jones, B. F., and Truesdell, A. H., 1976, WATEQF-A FORTRAN IV version of WATEQ, a computer program for calculating chemical equilibrium of natural waters: U.S. Geol. Survey Water Resources Inv., Rept. 76-13, 71 p.

Postma, D., 1977, The occurrence and chemical composition of recent Fe-rich mixed carbonates in a river bog: Jour. Sed. Petrology, v. 47, p. 1089-1098.

———— 1981, Formation of siderite and vivianite and the pore-water composition of a recent bog sediment in Denmark: Chem. Geology, v. 31, p. 225-244.

———— 1982, Pyrite and siderite oxidation in swamp sediments: Jour. Soil Sci., in press.

Pruden, G., and Bloomfield, C., 1968, The determination of iron (II) sulphide in soil in the presence of iron (III) oxide: Analyst, v. 93, p. 532-534.

Rickard, D. T., 1974, Kinetics and mechanism of the sulfidation of goethite: Am. Jour. Sci., v. 274, p. 941-952.

———— 1975, Kinetics and mechanism of pyrite formation at low temperatures: Am. Jour. Sci., v. 275, p. 636-652.

Rosenqvist, I. Th., 1970, Formation of vivianite in holocene clay sediments: Lithos, v. 3, p. 327-334.

Scheihing, M. H., Gluskoter, H. J., and Finkelman, R. B., 1978, Interstitial networks of kaolinite within framboids in the Meigs creek coal of Ohio: Jour. Sed. Petrology, v. 48, p. 723-732.

Suess, E., 1979, Mineral phases formed in anoxic sediments by microbial decomposition of organic matter: Geochim. et Cosmochim. Acta, v. 43, p. 339-352.

Sweeney, R. E., and Kaplan, I. R., 1973, Pyrite framboid formation: laboratory syntheses and marine sediments: Econ. Geology, v. 68, p. 618-634.

Tessenow, U., 1973, Lösungs-, Diffusions- und Sorptionsprozesse in der Oberschicht von Seesedimenten; II. Rezente Akkumulation von Eisen(II)phosphat (Vivianit) im Sediment eines meromiktischen Moorsees (Ursee, Hochschwarzwald) durch postsedimentäre Verlagerung: Arch. Hydrobiol. Suppl., v. 42, p. 143-189.

———— 1974, Lösungs-, Diffusions- und Sorptionsprozesse in der Oberschicht von Seesedimenten; IV. Reaktionsmechanismen und Gleichgewichte im System Eisen-Mangan-Phosphat im Hinblick auf die Vivianit-akkumulation im Ursee: Arch. Hydrobiol. Suppl., v. 47, p. 1-79.

Truesdell, A. H., and Jones, B. F., 1974, WATEQ, a computer program for calculating chemical equilibria in natural waters: U.S. Geol. Survey Jour. Research, v. 2, p. 233-248.

van Breemen, N., ms, 1976, Genesis and solution chemistry of acid sulfate soils in Thailand, Doctoral thesis, Wageningen Univ., 263 p.